Transcriptomic Analysis of Bone Marrow Adipose Tissue Reveals Enrichment in Lipid Transport in Response to Western Diet

Nicko Widjaja[1], Niki Jalava[1], Leena Strauss[1], Kirsi. A. Virtanen[2,3] and Kaisa K. Ivaska[1]*

[1]Institute of Biomedicine, University of Turku, Turku, Finland

[2]Turku PET Centre, University of Turku, Turku, Finland

[3]Turku PET Centre, Turku University Hospital, Turku, Finland

*Correspondence: Kaisa K. Ivaska (kaisa.ivaska@utu.fi). ORCID: 0000-0001-7482-7623.

Keywords: Bone marrow adipose tissue, white adipose tissue, high fat diet, transcriptomics, lipid metabolism.

Disclosure statement

The authors declare no competing interests.

Funding Information

This work is supported in part by Research Council of Finland (grant# 325498, K.K.I), Diabetes Wellness Finland (K.K.I), Laboratoriolääketieteen edistämissäätiö Foundation, Finland (K.K.I), Faculty of Medicine, University of Turku (K.K.I.), University of Turku Graduate

School (N.W., N.J.), Instumentarium Research Foundation (N.J.), Turku University Foundation (N.W.) and the Finnish Cultural Foundation Varsinais-Suomi Regional Fund (N.W., K.K.I.).

Abstract

Bone marrow adipose tissue (BMAT) is now recognised as a functional fat depot distinct from extramedullary white- (WAT) and brown (BAT) adipose tissues. BMAT expands in metabolic disorder such as obesity. However, the mechanism by which BMAT expands is less clear. Here, we present a comparative analysis of the transcriptomes of BMAT, WAT and BAT from 20-week-old Sprague-Dawley rats fed with chow diet (12%kJ fat) using bulk-RNA-sequencing. Gene-set enrichment analysis revealed over-representation of transcripts related to cellular proliferation and population of adipoprogenitor cells in BMAT. To further study BMAT expansion, we introduced a 12-week dietary intervention of Western diet (42%kJ fat). We first characterised obesity-related phenotypes such as adipocyte hypertrophy. Then, we compared the transcriptomes of femoral and tibial BMAT or gonadal WAT to the chow group. Western diet significantly increased bodyweight (P=0.02), whole-body fat percentage (P=0.009) and adipocyte size in humeral BMAT (P=0.02) and gonadal WAT (P=0.005), in comparison to the chow group. BMAT had a more robust transcriptomic response to Western diet than WAT. The transcriptome of BMAT was enriched in pathways related to lipid transport. In WAT, this enrichment was more related to lipid biosynthesis and modification. In summary, our data may suggest differences in the developmental maturity of BMAT relative to WAT and BAT in the chow group. Western diet induces differential responses in the transcriptomes of BMAT and WAT related to lipid homeostasis.

In BMAT, enrichment in the lipid transport pathways upon Western diet may suggest a role for BMAT in nutrient-sensing and lipid uptake.

1. Introduction

Bone marrow adipose tissue (BMAT) fills up to 70% of the bone marrow cavity in humans, comprising about 10% of our total fat mass [1–3]. BMAT is enriched in the long bones and is increased with ageing in both the axial and appendicular skeleton [2,4]. BMAT is now considered a fat depot distinct from white (WAT) and brown (BAT) adipose tissues [5]. We and others have shown that BMAT is a metabolically active fat depot [6–8]. BMAT may locally regulate haematopoiesis and bone remodelling within the local bone marrow microenvironment [9–11] or contribute to systemic metabolism via secreted factors [1,8,12]. The gene expression profile in BMAT differs from that of WAT and BAT in mice [13] and in humans [8,12], although it is less clear what these collective differences convey functionally. Further, the lipid metabolism in human BMAT appears to be different from WAT, with profound alterations in the lipolytic pathway [14].

Bone marrow is a complex tissue containing multiple cell types and extensive spatial heterogeneity [15]. Various stromal, non-adipocyte cells such as adipocyte precursor cells and the immune cells reside closely around or adjacently to bone marrow adipocytes (BMAds) [16–18], creating also challenges for the isolation of BMAds from bone marrow. In mice, BMAds originate from preadipocyte-like perivascular progenitors [19] and are mostly associated with sinusoidal vasculature [16]. Lineage tracing experiments in rodents have revealed two distinct stem cell-like adipogenic precursor populations, namely the

adipoprogenitor cells (APCs) and fate-committed preadipocytes, which are identified through different sets of enriched transcripts [20,21]. However, further characterisation for which population predominates at specific timepoints in bone marrow, or their relative abundance in different adipose tissue depots is less known.

BMAT is responsive to changes in metabolic status, such as during starvation or high-calorie intake, and the amount of BMAT fluctuates in most metabolic disorders in site-, age- and species-specific manners [4,21–23]. However, due to the challenges in accessing viable adipocytes from BMAT, little is known about how BMAds respond to metabolic stimuli in comparison to the classical white adipocytes at the cellular level. Further, the molecular mechanisms for BMAT expansion upon dietary challenge are mostly unknown and the limited data on nutrient-sensing pathways in BMAT comes from targeted analysis of mouse models [13,22,24]. We recently showed that BMAds expand in size in rats fed with high-fat, high-cholesterol Western diet for 24 weeks [6]. However, the molecular mechanisms driving the hypertrophy of BMAd are poorly understood. It is unclear whether BMAds respond to diet similarly to classical white adipocytes, *i.e.*, through hypertrophy, hyperplasia and inflammation [25]. The expansion of BMAds in rats upon Western diet was relatively stable and was not significantly affected by moderate lifestyle interventions such as a switch back to standard diet and running exercise [6]. Therefore, this study aimed to investigate the early changes in the transcriptomes of BMAT and WAT in response to Western diet at a shorter intervention period of 12 weeks.

We hypothesised that the physiological function of BMAT is impaired upon metabolic challenge, and the response to metabolic challenge is reflected in the transcriptomic

landscape of BMAds. Using bulk-RNA sequencing, here we report the transcriptomic characteristics enriched in BMAT isolated from femurs and tibiae of rat, in comparison to perigonadal and interscapular adipose tissues representing WAT and BAT, respectively. Next, we asked if the response to dietary challenge is different in BMAT and WAT. We used a 12-week intervention of high-fat, high-cholesterol Western diet and compared the diet-induced transcriptomic responses in BMAT and WAT. Finally, we uncovered biological pathways through targeted analysis of adipose tissue transcriptomes highlighting the differential response of BMAT and WAT to the dietary challenge.

2. Materials and methods

2.1 Animal experimentation

Eight-week-old male Sprague-Dawley rats (N=30) were purchased from the Central Animal Laboratory of the University of Turku, Finland, and allocated into two intervention groups of similar body weight at baseline (both groups averaged 286 g; $P>0.99$). Animals were fed with either standard chow diet (N=15, Envigo, USA; 0% cholesterol, 12.6 MJ/kg: 12% from fat, 22% from protein, 66% from carbohydrates), or Western diet (N=15, ssniff Spezialdiäten GmbH, Germany; 1.25% added cholesterol, 19.1 MJ/kg: 42% from fat, 15% from protein, 43% from carbohydrates) for 12 weeks. Three rats were housed in individual cages at standard condition of 12h light/dark cycle, 21°C and 55% humidity. Food and water were provided *ad libitum*. Food consumption was recorded by measuring the weight difference between the added and remaining food pellets three times a week. Using these data, energy consumption was recorded as kcal/cage. Body weight was measured weekly,

and body composition was measured with EchoMRI™ 1100 Analyzer (EchoMRI LLC, USA) at baseline and on intervention weeks 6 and 12. At the end of the 12-week dietary intervention, 20-week-old rats were sacrificed under terminal anaesthesia. Power calculations (n=15 animals/group) were based on our earlier pilot experiment in which the effect of Western diet on marrow adiposity was evaluated with histology, as described in section 2.5 (power 90%, α=0.05). The use of animals for experimentation was approved by the State Provincial Office of Southern Finland (ESAVI/30584/2022) and followed the Institutional Animal Care guidelines.

2.2 Collection of tissues

Samples (100-200 mg) of perigonadal WAT and interscapular BAT were dissected and snap-frozen in liquid nitrogen. BMAT was isolated from the marrow cavity of femur and tibia. In brief, metaphyseal ends of long bones were cut and bones were centrifuged at 1000x*g* for 30s to evacuate bone marrow content to a collection tube containing 1 mL HBSS buffer (Gibco, USA; supplemented with 10 mM HEPES, 2% BSA, 50 U/mL heparin, 1mM EDTA, 1 g/L L-glucose and 0.25% sodium citrate). The bottom layer of stromal-vascular fraction (SVF), mainly devoid of adipocytes, was collected for purity analysis. The top floating layer of BMAT-enriched fraction was next transferred onto a 10 µm cell strainer (PluriSelect, Germany) and centrifuged at 400x*g* at 4°C for 10 min to remove residual bone marrow cells that loosely attached to BMAT. SVF and BMAT-enriched samples were snap-frozen and all samples were stored at -80°C. The use of collagenase digestion to obtain more pure samples of BMAds was omitted, as recommended by recent guidelines from the International Bone Marrow Adiposity Society [26]. The presence of adipocytes in BMAT-

enriched sample was confirmed by staining for neutral lipids using 5 µg/mL BODIPY 493/503 (Invitrogen, USA) and for nucleus using 5 µg/mL HOECHST 33258 (Invitrogen, USA), and imaged with EVOS M5000 Imaging system (ThermoFischer Scientific, USA). In addition, intact humerus and samples of WAT, BAT and liver were collected for histology.

2.3 Total RNA extraction and gene expression analysis

Adipose tissue samples (WAT and BAT) were first homogenised with UltraTurrax T25 (Janke and Kunkel IKA-Labortechnik, Germany) in 5-second bursts at 9500 rpm on ice. The oil layer released from lysed adipocytes was discarded. Next, total RNA was extracted with TriSure (Bioline, UK) according to the manufacturer's protocol. For BMAT samples, RNA isolation with TriSure was followed by an additional column-based purification using RNeasy mini kit (QIAGEN, Germany) according to the manufacturer's protocol. RNA yield was evaluated with NanoDrop One C (ThermoFisher, USA), and RNA integrity number was obtained with 2100 Bioanalyzer (Agilent, USA). Total RNA (1 µg) was reverse transcribed to cDNA in a reaction mixture of Oligo(dT) (New England Biolabs, USA), dNTPs (ThermoFisher, USA), RNase inhibitor (Promega, USA) and Maxima Reverse Transcriptase (ThermoFisher, USA) with Mastercycler 5331 gradient (Eppendorf, USA).

Gene expression analysis with qPCR was performed with Bio-Rad CFX96 thermal cycler (Bio-Rad, USA) using 100 ng cDNA, 25 µM primers and Dynamo SYBR Green HS qPCR kit (ThermoFisher, USA) according to the manufacturer's protocol. Each primer sequence and target mRNA are listed in **Supplementary Table 1** [27]. Data was analysed by the Livak method [28] after normalising each mRNA expression to peptidylprolyl isomerase B (*Ppib*).

2.4 RNA-sequencing and transcriptomic analyses

A subset of five to six samples of WAT, BAT and BMAT was selected from both intervention groups (N= 15/group) for RNA-sequencing. As the mRNA expression of *Fabp4* has been shown to be upregulated in bone marrow by high-fat diet [29–31], the selection criteria included the response of BMAT to the diet as evaluated by mRNA expression of *Fabp4* by qPCR relative to the Chow group (+47%, $P<0.05$), and by acceptable RNA integrity number. Samples of WAT and BAT from the same animals were selected. mRNA library preparation, RNA sequencing and bioinformatic analyses were purchased from Novogene GmbH (Munich, Germany). Briefly, mRNA library was prepared with poly-A enrichment. Samples were then sequenced using Illumina NovaSeq 6000 with paired-end 150bp strategy and 20M reads per sample. For read alignment, HISAT2 algorithm was used to map the reads to *Rattus norvegicus* reference genome (mRatBN7.2). Variation in the transcript profile between samples and study groups was analysed with principal component analysis (PCA). Differentially expressed genes (DEGs) were identified with DESeq2 algorithm and shown visually as volcano plot or heatmap by transforming the data as log2-fold change (log2FC) or row z-score, respectively, on transcripts with $P<0.05$. The list of DEGs shown in each heatmap was sorted based on log2FC.

Next, we performed pathway-level gene-set enrichment analysis (GSEA, RRID: SCR_003199) with GSEA ver 4.4 [32]. Transcriptomic data was sorted by the signal-to-noise ratio metric and analysed based on gene sets from Gene Ontology (GO) terms. In rodents, adipocytes represent less than 50% of whole cell population in WAT, as sorted by recoverable nuclei in snRNAseq-based studies [33–35]. Given previous reports on the

differences in lipid metabolism between BMAT and WAT [14], we focused on the top 10 pathways related to lipid metabolism, by including in the analysis pathway names that contained the following keywords: 'adipo-', 'lipid', 'sterol' and 'fatty acid'. For GSEA statistics, enriched pathways with false discovery rate (FDR)<0.25 were considered statistically significant and set for further investigation of that gene set. A representative top-level pathway was chosen based on the occurrence of similar pathways from the top 10 pathways related to lipid metabolism. Finally, selected transcripts from that representative pathway were verified with qPCR, as described above, in BMAT and WAT from the whole cohort.

2.5 Histology

Samples of WAT, BAT and liver and intact humerus were fixed in 10% neutral-buffered formalin for 48 h. Humerus was decalcified with 10% EDTA, 1 M NaH_2PO_4, and 0.5 M Na_2HPO_4 for 16 days. Samples were paraffin-embedded, sectioned as 4 µm histological sections, stained with haematoxylin and eosin and scanned with Pannoramic P1000 (3DHistech, Hungary). Individual adipocyte area was semi-automatically measured using ImageJ (RRID: SCR_003070) from a single 1 mm x 1 mm region in WAT, annotated randomly, and in humeral bone marrow sections, annotated 5 mm distal from the proximal growth plate, as previously described [36]. Briefly, the script targets the delipidated region of adipocytes between 200 μm^2 and 4000 μm^2 for BMAds, or between 300 μm^2 and 9000 μm^2 for white adipocytes (WAds). Individual adipocyte size distribution was plotted according to bin width of 200 μm^2 and 600 μm^2 for BMAds and WAds, respectively. The accumulation of lipid droplets in hepatocytes was quantitated from the whole slide images of HE-stained

histological liver sections with deep learning-based image analysis model utilising Aiforia Create cloud platform version 5.3 (Aiforia technologies, Finland; RRID: SCR_022739), as previously described [37]. Briefly, the area for microvesicular or macrovesicular steatosis was based on the detection of lipid droplet with a diameter less than or more than 6 µm, respectively, within the hepatocytes.

2.6 Blood samples

Blood samples were collected into lithium heparin-containing tubes with a cardiac puncture at the time of sacrifice. Blood samples were immediately centrifuged at 200x*g* for 10 min to obtain plasma samples and stored at -80°C until analysis. Plasma glucose levels were measured using Glucose Assay Kit (STA-681, Cell Biolabs Inc, USA) and total and free cholesterol was measured with Cholesterol Quantification Assay Kit (CS0005, Sigma-Aldrich, Germany) according to the manufacturers' instructions. Measurements were performed with EnSight multimode plate reader (Revvity Oy, Finland).

2.7 Bone microarchitecture and bone mineral density

Humeral length was measured with a calliper. Humerus was scanned with µCT SkyScan 1272 (Bruker, USA) at 70 kV, 142 µA and a spatial voxel resolution of 10 µm. The growth plate at the proximal humeral metaphysis was located as a reference point for the analysis of the trabecular region, which spanned 2 mm distally. Next, the most distal region of deltoid tuberosity was selected as a reference point for the analysis of the cortical region, which spanned 1 mm distally. Bone mineral density was measured by referencing the attenuation coefficient of each region to that of phantom materials with known density.

2.8 Statistical analysis

Data are presented as box plots represent median value with interquartile range and whiskers represent minimum and maximum values, whenever applicable. Each data set was first tested for normal distribution with Shapiro-Wilk normality test. Groupwise mean comparison was performed with Student's t-test for normally distributed data or Mann-Whitney U-test for non-normally distributed data. *P*-values< 0.05 were considered statistically significant. Correlation coefficient R was computed with Pearson or Spearman correlation test for normally or non-normally distributed data, respectively. For qPCR analysis of adipose tissue comparison, one-way ANOVA with Dunnett's correction for multiple comparisons was performed. For adipocyte size distribution analysis, two-way ANOVA with Sidak's correction for multiple comparisons was performed. Adjusted *P*-values< 0.05 were considered statistically significant. To reduce bias, data collection was performed using unique identifiers blinded to the experimental group.

For RNAseq data, *P*-values and adjusted *P*-values or FDR were computed in DESeq2 and GSEA software. Adjusted *P*-values (P_{adj}) < 0.05 or FDR< 0.25 were considered statistically significant. Statistical analyses and graphing were performed in GraphPad Prism 10.6.1 (Graphpad Software LLC, USA).

3. Results

3.1 Western diet results in metabolic and skeletal changes in rats

Rats with the 12-week dietary intervention had significantly higher body weight (mean +7.1%, *P*=0.02; **Fig. 1A**), weight gain (+18.1%, *P*<0.001; **Fig. 1B**) and whole-body fat percentage (+33.2%,

P=0.009; **Fig. 1C**) in comparison to the chow group. On average, rats fed with Western diet had persistently lower food consumption by weight than chow diet, despite having higher energy intake when adjusted for metabolizable energy of each diet component (*P*<0.05, data not shown). Total plasma cholesterol was significantly higher in the Western diet group than in the chow group (+20.4%, *P*=0.002; **Fig. 1D**), but there was no difference in plasma glucose levels (-1.76%, *P*=0.34; **Fig. 1E**). We found significantly larger areas of microsteatotic and macrosteatotic lesions in the liver samples of the Western diet group compared to the chow group (both *P*<0.001; **Fig. 1F**). Further, we observed changes in humeral trabecular region (**Fig. 1G**) as reflected by the significantly higher trabecular separation (+36.3%, *P*=0.001; **Fig. 1H**) and lower trabecular number (-10.9%, *P*=0.002; **Fig. 1I**) and trabecular connectivity density (Conn.D, -20.5%, *P*=0.009; **Table 1**) in rats fed with Western diet. Bone mineral density in both trabecular and cortical regions was not significantly affected by Western diet (all *P*>0.05; **Table 1)**.

3.2 BMAT is distinct from WAT and BAT and is enriched in pathways and transcripts related to the proliferation of adipoprogenitor cells

First, we compared transcriptomes of three adipose depots in chow-fed rats, *i.e.,* without dietary challenge. The collected BMAT-enriched fractions were positive for neutral lipid and nuclear staining (**Fig. 2A**) and expressed significantly more mRNA for adipocyte-related markers perilipin-1 (*Plin1*) and *Adipoq,* and they expressed significantly less haematopoietic-related markers integrin alpha M (*Itgam*) and protein tyrosine phosphatase receptor (*Ptprc*) compared to SVF (**Fig. 2B**), highlighting the enrichment of adipocytes in BMAT samples. BMAT expressed significantly less mRNA for adipocyte-related markers *Adipoq, Fabp4,* cluster of differentiation 36 (*Cd36*) and *Leptin* in comparison to WAT and BAT (all *P*<0.05; **Fig. 3A**). PCA of the entire RNAseq data revealed three separate clusters

representing BMAT, WAT and BAT transcriptomes (**Fig. 3B**). In BMAT, GSEA revealed the top 10 enriched pathways, *e.g.,* spliceosome- and chromatin-related complexes, *i.e.,* processes that are tied to cellular proliferation (**Supp. Figs. 1A and B**) [27]. In WAT, Pathways related to lipid metabolism (*e.g.,* GO terms fatty acid beta-oxidation and fatty acid catabolism) and extracellular matrix (*e.g.,* extracellular matrix organisation, basement membrane and collagen trimer) were enriched (**Supp. Fig. 1A**), while those related to oxidative phosphorylation and mitochondrial energy metabolism were enriched in BAT (**Supp. Fig. 1B**). To highlight pathways that were enriched by the contribution of adipocytes within each adipose tissue sample, we further filtered the results using the predefined adipocyte physiology pathway-set, as described in detail above. In BMAT, pathways related to membrane-lipid processes (*e.g.,* phospholipid scrambling and lipid phosphorylation; all FDR<0.25) were more enriched when compared to WAT (**Fig. 3C**) and BAT (**Fig. 3D**). Whereas in WAT and BAT, pathways related to adipocyte physiology (*e.g.,* fatty acid beta oxidation, fatty acid metabolic process and lipid droplet; all FDR<0.25) were more enriched than in BMAT (**Figs. 3C and D**).

The top enrichments in BMAT that were related to cell proliferation and membrane-lipid processes led us to further investigate transcripts related to less-differentiated adipocyte populations in BMAT. Using previously published lists of transcripts [20] known to be enriched in the adipoprogenitor cells (APCs) and pre-adipocyte population, we found in BMAT an abundance of transcripts related to the APCs, but not pre-adipocytes, when compared to WAT and BAT (**Fig. 3E**). qPCR analysis of the entire chow-fed cohort (N=15) confirmed that the transcripts related to APCs, *e.g.,* stem cells antigen-1 (*Sca1*), matrix metalloproteinase-

9 (*Mmp9*) and oncostatin M (*Osm*), were expressed at significantly higher levels in BMAT when compared to WAT and BAT (all $P<0.01$, **Fig. 3F**). In contrast, transcripts related to more mature pre-adipocytes, *e.g.,* prolactin receptor (*Prlr*), and quinolinate phosphoribosyltransferase (*Qprt*), were expressed at lower levels in BMAT than in WAT and BAT (**Fig. 3G**).

3.3 Western diet induces hypertrophy in both BMAds and WAds

Next, we evaluated changes in the morphology of adipocytes in response to the 12-week Western diet intervention. On average, BMAds were smaller than WAds. Histological analysis of individual adipocyte size revealed that Western diet significantly enlarged the size of BMAds (averaged 822 μm^2 versus 681 μm^2, +20.7%, $P=0.02$; **Fig. 4A**) in the proximal BM of the humerus. The average number of BMAds in the Western diet group (292 BMAds per ROI) was similar to that in the chow group (277 BMAds, $P=0.70$). In line with this, the frequency of small BMAds, particularly those sized< 400 μm^2, was significantly less in the Western diet group compared to the chow group ($P<0.001$; **Fig. 4B**). Similarly, Western diet significantly enlarged the size of WAds in WAT (2399 μm^2 versus 1958 μm^2, +22.5%, $P=0.005$; **Fig. 4C**). The frequency of small adipocytes sized< 900 μm^2 was significantly less in rats fed with Western diet ($P<0.001$; **Fig. 4D**). In addition, the size of BMAds, but not WAds, was inversely correlated to trabecular bone volume fraction (Tb.BV/TV, R=-0.48, $P=0.04$) and trabecular number (Tb.N, R=-0.67, $P=0.002$; **Table 1**).

3.4 The hypertrophic response of BMAds to Western diet is associated with the enrichment in pathways related to lipid transport

To understand the molecular mechanism driving the hypertrophy of BMAds upon Western diet, we compared BMAT transcriptomes in rats fed with either chow or Western diet. PCA revealed two separate clusters of transcriptomes, corresponding to the chow and Western diet groups (**Fig. 5A**). Further, we identified 3278 DEGs (N=889 after statistical adjustment), of which 1513 (46%) were upregulated (N=335; 38%) and 1765 (54%) were downregulated (N=554; 62%) (**Fig. 5B**). In GSEA, we first focused on pathways related to lipid metabolism. The fatty acid derivative biosynthetic process (accession number GO:1901570; FDR=0.01) was the top enriched pathway in BMAT in response to Western diet. Consistently, several pathways related to lipid transport appeared to be enriched with Western diet, such as lipid translocation (GO:0034204; FDR=0.04), regulation of membrane lipid distribution (GO:0097035; FDR=0.07), phospholipid transport (GO:0015914; FDR=0.12) and intracellular lipid transport (GO:0032365; FDR=0.25; **Fig. 5C**). Based on the enrichment related mainly to the lipid transport, we discovered four core-enriched transcripts annotated in the lipid transport pathway (GO:0006869), including *Cd36,* ATP-binding cassette sub-family G member 1 (*Abcg1*), *Fabp4* and acyl-coA synthetase long-chain family member 4 (*Acsl4*). Using qPCR analysis from the entire animal cohort, we verified in BMAT a significant upregulation in the expression levels of *Abcg1* (+32%, *P*=0.03) and *Fabp4* (+47%, *P*=0.03), and an increasing, but not significant, trend for the expression of *Cd36* (+63%, *P*=0.17) and *Acsl4* (+44%, *P*=0.36) in response Western diet (**Fig. 5E**). In WAT,

Western diet did not significantly affect these selected transcripts (all $P>0.05$) related to lipid transport, except for *Abcg1* (+31%, $P=0.02$; **Fig. 5F**).

We then evaluated GSEA on a global level without data filtering **(Figs. 6A and B)**. In BMAT, the top 10 GSEA enriched by Western diet revealed significant enrichments (all FDR<0.25) in pathways related to the immune system process, *e.g.,* cytokine receptor activity (GO:0004896) and antigen processing and presentation of exogenous peptide via MHC class II (GO:0019886; **Fig. 6A**). To better understand the putative inflammatory response in BMAT to Western diet, we queried DEGs (all $P<0.05$) in our dataset which are annotated in the GO database for the immune system process (GO:0002376). Western diet significantly increased the expression of several transcripts related to adipose tissue inflammation [38], such as monocyte chemoattractant protein-1 (*Mcp1,* also known as *Ccl2*), Lipocalin-2 (*Lcn2*), C-C chemokine receptor type 2 (*Ccr2*), interleukin 1-beta (*Il1b*) and interleukin-6 (*Il6*) **(Fig. 6C)**. Upregulation of these transcripts was further verified in the entire cohort with qPCR, and we saw a significant upregulation of *Mcp1* (+114%; $P=0.01$) and *Lcn2* (+81%; $P=0.05$) in BMAT upon Western diet (**Fig. 6D**). similar upregulation was not seen in WAT (**Fig 6E**).

3.5 The hypertrophic response of WAds to Western diet is associated with the enrichment in pathways related to lipid biosynthesis and modification

Similar to the analysis of BMAT, we performed bulk-RNA-sequencing from samples of gonadal WAT in rats fed with either chow or Western diet. PCA revealed a less pronounced separation in the transcriptome clusters of WAT between diet groups (**Fig. 7A**). We further found only 1633 DEGs (N=82 after statistical adjustment), compared to 3278 DEGs in BMAT, of which 848 (52%) were

upregulated (N=32; 39%) and 785 (48%) were downregulated (N=50; 61%) (**Fig. 7B**). The overall top 10 GSEA showed significant enrichments (all FDR< 0.25) in pathways related to translation and protein synthesis, *e.g.*, cytosolic ribosome (GO:0022626) and ribosomal subunit (GO:0044391; **Fig. 6B**). When we focused the GSEA analysis on pathways related to lipid metabolism, we observed that several pathways related to lipid biosynthesis and modification, such as those involved in the cholesterol and fatty acid biosynthesis, were enriched in WAT with Western diet (**Fig. 7C**). Based on the enrichments in lipid biosynthesis in WAT, we selected representative transcripts stearoyl-CoA desaturase-1 and -2 (*Scd1* and *Scd2*), patatin-like phospholipase domain-containing protein 3 (*Pnpla3*) and lipin-3 (*Lpin3*) from the lipid biosynthetic process (GO:0008610; **Fig. 7D**), and verified the expression in WAT and BMAT with qPCR. In WAT, we observed significant upregulation of *Scd1* (35-fold increase, $P<0.001$), Scd2 (+93%, $P<0.001$) and *Pnpla3* (+69%; $P=0.008$) with Western diet, but not *Lpin3* (**Fig. 7E**). In BMAT, we observed a modest but significant upregulation only for Scd1 (2.3-fold; $P=0.005$; **Fig. 7F**). Under normal conditions, *i.e.,* study group without Western diet, the mRNA expression of *Scd1* was significantly lower in BMAT than WAT (12-fold, $P< 0.001$). There were also some similarities in the response of WAT and BMAT to Western diet. For instance, the pathway entitled response to fatty acid (GO:0070542) was among the top 10 pathways of adipocyte physiology in both BMAT (**Fig. 5C**) and WAT (**Fig. 7C**) in response to Western diet.

4. Discussion

In this study, we compared the transcriptomes of three adipose tissue depots of BMAT, WAT and BAT in rats, and studied the effect of high-fat, high-cholesterol Western diet on BMAT and WAT. Our data demonstrates that BMAT is transcriptionally different from WAT and BAT, and is enriched in transcripts related to the proliferation of less-mature APCs. BMAT and WAT show differential transcriptomic response to Western diet. The hypertrophy

of BMAds is more related to the enrichment in pathways related to lipid transport, while the hypertrophy of WAds is more related to pathways involved in lipid biosynthesis and modification.

BMAT isolated from rat femur and tibia expressed adipocyte-related transcripts, *e.g.*, *Adipoq*, *Fabp4* and *Leptin* at significantly lower level than WAT and BAT, similar to what others have observed in rodents [13,24]. On a pathway-level, our results showed enrichment in pathways related to proliferation and phospholipid scrambling, which may suggest active cellular division. To identify the potential proliferating cell population, we further analysed the transcriptome for the presence of APCs and pre-adipocytes that spatially associate with mature BMAds [16–18]. Using curated lists of transcripts defining murine skeletal *Sca1*$^{+}$ stem cell-like populations in bone marrow [20], we observed abundance of several transcripts related to APCs. Among those, *Mmp9*, a matrix metalloproteinase, has been shown to be expressed abundantly in undifferentiated pre-adipocytes in rodents [20,39] and humans [40,41], and found to be inversely associated with adipogenic maturation [41]. *Osm* was highly upregulated in our dataset and it has been reported to inhibit adipogenesis progression in rodents [42]. Collectively, our data may suggest that BMAT is a less mature adipose tissue than WAT and BAT, at least in young rats on standard diet, or that BMAd progenitors are transcriptionally distinct from those for white and brown adipocytes. This is in line with studies reporting the continuous BMAT expansion during ageing in rodents [5,24,43–45]. The physiological significance for the relatively abundant presence of APCs in BMAT is presently unknown, and therefore warrants more investigation.

We found that hypertrophy of BMAds and WAds in response to the dietary intervention occurs, at least in part, via different pathways. This is highlighted by the enrichment of different transcripts in these two different adipose tissue types. In BMAT, we observed enrichment in transcripts related to lipid transport. Bone marrow is a highly perfused organ in the haematopoietic-rich femoral red marrow, receiving higher perfusion than subcutaneous WAT [46]. Further, we and others have earlier reported lipid and fatty acid uptake in adipocyte-rich bone marrow of long bones [7,47,48]. Collectively, this may suggest a nutrient-sensing role for BMAT in clearing circulating lipids. Interestingly, our data did not show significant changes in transcripts for the classical adipocyte machinery for lipid uptake, including the fatty acid transfer proteins (*Fatps*) family and lipoprotein lipase (*Lpl*), suggesting other mechanisms responsible for fatty acid uptake in BMAds. Bartelt and colleagues have shown increased fatty acid uptake in the bone marrow of adipocyte-specific *Lpl*$^{-/-}$ mice, and they implied an LPL-independent hydrolysis of fatty acids for uptake in BMAds [47]. We observed increases in the expression of *Cd36* and *Fabp4* which are known to channel fatty acids into adipocytes and traffic them for storage. Notably, CD36 is known to channel up to 50% of fatty acids into 3T3-L1 adipocytes through caveolar endocytosis [49]. Accordingly, our RNAseq data shows modest upregulation for machineries downstream of CD36-mediated fatty acid uptake, including Lck/Yes novel tyrosine kinase (*Lyn*), Zinc Finger DHHC-type palmitoyltransferase 5 (*Zdhhc5*), Acyl-protein thioesterase 1 (*Lypla1*) and Spleen-associated tyrosine kinase (*Syk*) (data not shown). Regardless, detailed investigation on the mechanisms of lipid uptake in BMAds remain to be comprehensively studied.

Our data shows differential transcriptomic response between BMAT and WAT upon Western diet. In WAT we observed enrichment in the transcripts related to lipid biosynthesis, including intracellular lipid processing and modification. In particular, *Scd1,* the rate-limiting enzyme responsible the synthesis of mono-unsaturated fatty acids (MUFAs) [50] was strikingly upregulated in WAT (35-fold) but only modestly in BMAT (2.3-fold). Such contrast further highlights the differential responses of BMAT and WAT to Western diet. In *Scd1*$^{-/-}$ mice, Ntambi and colleagues showed marked reduction in triglyceride synthesis [51], thereby extending the role of *Scd1* beyond fatty acid desaturation and likely potentiate lipid storage and adipocyte hypertrophy in WAds. To clarify the term lipid biosynthesis, our data did not show enrichment in pathways related to carbohydrate handling in WAT nor BMAT, such as carbohydrate kinase activity (GO:0019200) and carbohydrate transmembrane transport (all FDR> 0.25, data not shown), as adipocytes may accrue lipids through *de novo* lipogenesis from carbohydrate precursors. Further, we and others have shown suppressed glucose uptake in bone marrow and WAT in response to high fat diet [6,52,53], making *de novo* lipogenesis unlikely in explaining lipid droplet growth apart from lipid uptake. Further, we observed a similar enrichment in the GO term response to fatty acids (GO:0070542) in both BMAT and WAT in response to Western diet, supporting the nutrient-sensing role of both adipose tissues. However, this is followed by a differential response of lipid transport in BMAT and lipid biosynthesis and processing in WAT.

Interestingly, our data shows enrichment in pathways related to the immune system processes in BMAT in response to Western diet, which was not as pronounced in WAT. We further verified the significant upregulation of pro-inflammatory cytokines, such as *Mcp1*

and *Lcn2*, in BMAT by Western diet. Our data is not in line with the previously reported non-inflammatory phenotype of BMAT in mice upon 60 kcal% HFD [13], suggesting perhaps a species-specific difference in the inflammatory response of BMAT upon HFD. In humans, on the other hand, Fazeli and colleagues reported an increase in pro-inflammatory transcripts in mature primary BMAds upon acute high-calorie feeding [54]. Studies on changes related to the inflammation status tied to the expansion of BMAT upon Western diet in different species are therefore warranted.

We also observed a significant, inverse associations between the size of BMAds and trabecular bone microstructure, both assessed in humerus, which is in line with what we and others have reported in tibia in rodents fed with high-fat diet [6,13,55,56]. However, the causal relationship between bone loss and bone marrow adiposity has yet to be determined, particularly as context-dependent bone loss may occur independently from BMAT expansion [57–59]. Further, a supportive role of BMAds in bone formation has also been reported [10,60]. Future work is needed to examine whether BMAds in the humerus follow the pattern of adipocyte heterogeneity in the tibia [61], and whether BMAds expansion alone or in combination with changes in bone marrow environment upon Western diet potentiates trabecular bone loss.

The present study is not without limitations. We analysed samples of BMAT from femur and tibia, WAT from perigonadal region and BAT from interscapular region, from male Sprague-Dawley rats, at 20 weeks of age. Adipose tissues exhibit depot- and sex-specific and age-dependent characteristics [36,43,45,62], thereby limiting interpretation of the data to other specific adipose depots or animals of different age. Regardless, femoral and tibial BMAT

represent two very well characterised subpopulations of BMAds, providing a holistic overview of the response of BMAT to Western diet. Further, gonadal WAT used in this study has commonly been used as a surrogate for visceral fat depot that responds to obesogenic feeding, offering a practical and metabolically informative site for assessing adiposity in response to dietary intervention [63]. Despite efforts to deplete SVF from our samples of BMAT, other non-adipocyte cells may have remained attached with BMAds and carried over to the analysis. We acknowledge that the estimation of cellularity of the samples (adipocytes vs. other cell types) via, *e.g.*, cell sorting, was not evaluated in the present study and it should be addressed in future studies. Further, the results of bulk RNA-sequencing data reflect changes captured at a tissue level, thereby, to some extent, our results may have been contributed by non-adipocyte cells in the samples. To address this, we employed a targeted analysis through stringent data filtering which enabled us to focus specifically on pathways related to lipid metabolism. The omission of collagenase digestion, as recommended by the recent guidelines [26], enabled us to preserve the amount of BMAT and to perform RNAseq on individual samples, which is not always feasible for the challenging isolation of BMAT from rodents [43,64]. The strengths of the study include global analysis on adipose tissue transcriptomes, which was further verified by qPCR on selected genes from the whole study cohort. In the future, the use of single-nucleus RNA-sequencing should enable the investigation up to cellular resolution, although the mRNA expression can also differ between nuclei and cytoplasm, further complicating the interpretation of the data [65]. However, transcriptomic analyses alone cannot fully confirm differences in progenitor cells or metabolic functions. In addition, the use of Western diet

allowed us to improve the translatability and clinical relevance of the results, as Western diet may mirror the gradual development of obesity in humans [66]. The ongoing development for the ex vivo cultures for primary BMAds [26] should allow us to further investigate the lipid uptake mechanism in BMAds in the future.

In summary, we present herein the global transcriptomic analysis of three adipose tissue depots of BMAT, WAT and BAT. Our data suggests that less-mature APCs are over-represented in BMAT, possibly reflecting the developmental maturity of BMAT. The expansion of BMAT involves, in parts, pathways related to lipid transport while the expansion of WAT may rely more on pathways involved in lipid biosynthesis and modification. Further, BMAT appears to be more responsive to the diet-induced transcriptomic changes than WAT. Collectively, the present study strengthens the concept of BMAT as a distinct adipose depot and provides new information on the enriched pathways in BMAT responding to dietary intervention.

CRediT authorship contribution statement

Nicko Widjaja: Conceptualization, Methodology, Validation, Formal analysis, Investigation, Writing - Original Draft, Writing - Review & Editing, Visualization, Funding acquisition.

Niki Jalava: Conceptualization, Methodology, Investigation, Writing - Review & Editing, Funding acquisition

Leena Strauss: Formal Analysis, Writing - Review & Editing

Kirsi A. Virtanen: Writing - Review & Editing, Supervision

Kaisa K. Ivaska: Conceptualization, Methodology, Resources, Writing - Original Draft, Writing - Review & Editing, Supervision, Project administration and Funding acquisition.

Funding sources

This work is supported in part by Research Council of Finland (grant# 325498, K.K.I), Diabetes Wellness Finland (K.K.I), Laboratoriolääketieteen edistämissäätiö Foundation, Finland (K.K.I), Faculty of Medicine, University of Turku (K.K.I.), University of Turku Graduate School (N.W., N.J.), Instumentarium Research Foundation (N.J.), Turku University Foundation (N.W.) and the Finnish Cultural Foundation Varsinais-Suomi Regional Fund (N.W., K.K.I.).

Declaration of competing interest

The authors declare no competing interests.

Acknowledgements

The authors thank Laura Mairinoja for the assistance in the analysis of liver histology, and Henna Karhunen and Milja Arponen for their excellent technical assistance. Personnel of the Central Animal Laboratory at the University of Turku is acknowledged for their technical

assistance with animal maintenance and handling. We thank the Histology core facility of the Institute of Biomedicine, University of Turku, Finland for their assistance in histological tissue processing. Scientific illustrations are provided by Servier Medical Art (https://smart.servier.com), licensed under CC BY 4.0 (https://creativecommons.org/licenses/by/4.0/).

Data availability

Original data generated and analyzed during this study are included in this published article or in the data repositories listed in References. The raw datasets generated and analyzed during this study are publicly available in Zenodo at https://doi.org/10.5281/zenodo.21023939

References

1. Cawthorn WP, Scheller EL, Learman BS, Parlee SD, Simon BR, Mori H. Bone marrow adipose tissue is an endocrine organ that contributes to increased circulating adiponectin during caloric restriction. *Cell Metab*. 2014;20(2):368-375. Accessed September 8, 2023. https://www.sciencedirect.com/science/article/pii/S155041311400268X

2. Karampinos DC, Ruschke S, Dieckmeyer M, Diefenbach M, Franz D, Gersing AS, Krug R, Baum T. Quantitative MRI and spectroscopy of bone marrow. *Journal of Magnetic Resonance Imaging*. 2018;47(2):332-353. doi:10.1002/jmri.25769

3. Blebea JS, Houseni M, Torigian DA, Fan C, Mavi A, Zhuge Y, Iwanaga T, Mishra S, Udupa J, Zhuang J, Gopal R, Alavi A. Structural and Functional Imaging of Normal Bone Marrow and Evaluation of Its Age-Related Changes. *Semin Nucl Med*. 2007;37(3):185-194. doi:10.1053/j.semnuclmed.2007.01.002

4. Xu W, Mesa-Eguiagaray I, Morris DM, Wang C, Gray CD, Sjöström S, Papanastasiou G, Badr S, Paccou J, Li X, Timmers PRHJ, Timofeeva M, Farrington SM, Dunlop MG, Semple SI, MacGillivray T, Theodoratou E, Cawthorn WP. Deep learning and genome-wide association meta-analyses of bone marrow adiposity in the UK Biobank. *Nature Communications 2024 16:1*. 2025;16(1):99-. doi:10.1038/s41467-024-55422-4

5. Hardouin P, Rharass T, Lucas S. Bone Marrow Adipose Tissue: To Be or Not To Be a Typical Adipose Tissue? *Front Endocrinol*. 2016;7:85. doi:10.3389/fendo.2016.00085

6. Ojala R, Widjaja N, Hentilä J, Jalo A, Helin JS, Nissinen TA, Jalava N, Eskola O, Rajander J, Löyttyniemi E, Ivaska KK, Hannukainen JC. Evaluation of bone marrow glucose uptake and adiposity in male rats after diet and exercise interventions. *Front Endocrinol (Lausanne)*. 2024;15:1422869. doi:10.3389/fendo.2024.1422869

7. Ojala R, Motiani KK, Ivaska KK, Arponen M, Eskelinen JJ, Virtanen KA, Löyttyniemi E, Heiskanen MA, U-Din M, Nuutila P, Kalliokoski KK, Hannukainen JC. Bone Marrow Metabolism Is Impaired in Insulin Resistance and Improves After Exercise Training. *J Clin Endocrinol Metab*. 2020;105(12):e4290-e4303. doi:10.1210/clinem/dgaa516

8. Pham TT, Ivaska KK, Hannukainen JC, Virtanen KA, Lidell ME, Enerbäck S. Human Bone Marrow Adipose Tissue is a Metabolically Active and Insulin-Sensitive Distinct Fat Depot. *J Clin Endocrinol Metab*. 2020;105(7):2300-2310. doi:doi:10.1210/clinem/dgaa216

9. Li Z, Bagchi DP, Zhu J, Bowers E, Yu H, Hardij J, Mori H, Granger K, Skjaerlund J, Mandair G, Abrishami S, Singer K, Hankenson KD, Rosen CJ, MacDougald OA. Constitutive bone marrow adipocytes suppress local bone formation. *JCI Insight*. 2022;7(21). doi:10.1172/JCI.INSIGHT.160915

10. Li Z, Bowers E, Zhu J, Yu H, Hardij J, Bagchi DP, Mori H, Lewis KT, Granger K, Schill RL, Romanelli SM, Abrishami S, Hankenson KD, Singer K, Rosen CJ, Macdougald OA. Lipolysis of bone marrow adipocytes is required to fuel bone and the marrow niche during energy deficits. *Elife*. 2022;11. doi:10.7554/ELIFE.78496

11. Peng H, Hu B, Xie LQ, Su T, Li CJ, Liu Y, Yang M, Xiao Y, Feng X, Zhou R, Guo Q, Zhou HY, Huang Y, Jiang TJ, Luo XH. A mechanosensitive lipolytic factor in the bone marrow promotes osteogenesis and lymphopoiesis. *Cell Metab*. 2022;34(8):1168-1182.e6. doi:10.1016/j.cmet.2022.05.009

12. Suchacki KJ, Tavares AAS, Mattiucci D, Scheller EL, Papanastasiou G, Gray C, Sinton MC, Ramage LE, McDougald WA, Lovdel A, Sulston RJ, Thomas BJ, Nicholson BM, Drake AJ, Alcaide-Corral CJ, Said D, Poloni A, Cinti S, Macpherson GJ, Dweck MR, Andrews JPM, Williams MC, Wallace RJ, van Beek EJR, MacDougald OA, Morton NM, Stimson RH, Cawthorn WP. Bone marrow adipose tissue is a unique adipose subtype with distinct roles in glucose homeostasis. *Nat Commun*. 2020;11(1):3097. doi:10.1038/s41467-020-16878-2

13. Tencerova M, Figeac F, Ditzel N, Taipaleenmäki H, Nielsen TK, Kassem M. High-Fat Diet-Induced Obesity Promotes Expansion of Bone Marrow Adipose Tissue and Impairs Skeletal Stem Cell Functions in Mice. *J Bone Miner Res*. 2018;33(6):1154-1165. doi:10.1002/jbmr.3408

14. Attane C, Esteve D, Chaoui K, Iacovoni JS, Corre J, Moutahir M, Valet P, Schiltz O, Reina N, Muller C. Human Bone Marrow Is Comprised of Adipocytes with Specific Lipid Metabolism. *Cell Rep*. 2020;30(4):949-958. doi:10.1016/j.celrep.2019.12.089

15. Bandyopadhyay S, Duffy MP, Ahn KJ, Sussman JH, Pang M, Smith D, Duncan G, Zhang I, Huang J, Lin Y, Xiong B, Imtiaz T, Chen CH, Thadi A, Chen C, Xu J, Reichart M, Martinez Z, Diorio C, Chen C, Pillai V, Snaith O, Oldridge D, Bhattacharyya S, Maillard I, Carroll M, Nelson C, Qin L, Tan K. Mapping the cellular biogeography of human bone marrow niches using single-cell transcriptomics and proteomic imaging. *Cell*. 2024;187(12):3120-3140.e29. doi:10.1016/j.cell.2024.04.013

16. Robles H, Park S, Joens MS, Fitzpatrick JAJ, Craft CS, Scheller EL. Characterization of the bone marrow adipocyte niche with three-dimensional electron microscopy. *Bone*. 2019;118:89-98. doi:10.1016/j.bone.2018.01.020

17. Matsushita Y, Ono W, Ono N. Toward Marrow Adipocytes: Adipogenic Trajectory of the Bone Marrow Stromal Cell Lineage. *Front Endocrinol (Lausanne)*. 2022;13. doi:10.3389/fendo.2022.882297

18. Robino JJ, Pamir N, Rosario S, Crawford LB, Burwitz BJ, Roberts CT, Kurre P, Varlamov O. Spatial and biochemical interactions between bone marrow adipose tissue and hematopoietic stem and progenitor cells in rhesus macaques. *Bone*. 2020;133:115248. doi:10.1016/j.bone.2020.115248

19. Zhong L, Yao L, Tower RJ, Wei Y, Miao Z, Park J. Single cell transcriptomics identifies a unique adipose lineage cell population that regulates bone marrow environment. *Elife*. 2020;9.

20. Ambrosi TH, Scialdone A, Graja A, Gohlke S, Jank AM, Bocian C, Woelk L, Fan H, Logan DW, Schürmann A, Saraiva LR, Schulz TJ. Adipocyte Accumulation in the Bone Marrow during Obesity

and Aging Impairs Stem Cell-Based Hematopoietic and Bone Regeneration. *Cell Stem Cell*. 2017;20(6):771-784.e6. doi:10.1016/j.stem.2017.02.009

21. Ambrosi TH, Taheri S, Chen K, Sinha R, Wang Y, Hunt EJ, Goodnough LH, Murphy MP, Steininger HM, Hoover MY, Felix F, Weldon KC, Koepke LS, Sokol J, Liu DD, Zhao L, Conley SD, Lu WJ, Morri M, Neff NF, Van Rysselberghe NL, Wheeler EE, Wang Y, Leach JK, Saiz A, Wang A, Yang GP, Goodman S, Bishop JA, Gardner MJ, Wan DC, Weissman IL, Longaker MT, Sahoo D, Chan CKF. Human skeletal development and regeneration are shaped by functional diversity of stem cells across skeletal sites. *Cell Stem Cell*. 2025;32(5):811-823.e11. doi:10.1016/J.STEM.2025.02.013

22. Rosen CJ, Horowitz MC. Nutrient regulation of bone marrow adipose tissue: skeletal implications of weight loss. *Nat Rev Endocrinol*. 2023;19(11):626-638. doi:10.1038/s41574-023-00879-4

23. Badr S, Cotten A, Lombardo D, Ruschke S, Karampinos DC, Ramdane N, Genin M, Paccou J. Bone Marrow Adiposity Alterations in Postmenopausal Women With Type 2 Diabetes Are Site-Specific. *J Endocr Soc*. 2024;8(11). doi:10.1210/JENDSO/BVAE161

24. Liu LF, Shen WJ, Ueno M, Patel S, Kraemer FB. Characterization of age-related gene expression profiling in bone marrow and epididymal adipocytes. *BMC Genomics*. 2011;12:212. doi:10.1186/1471-2164-12-212

25. Sun K, Kusminski CM, Scherer PE. Adipose tissue remodeling and obesity. *Journal of Clinical Investigation*. 2011;121(6):2094-2101. doi:10.1172/JCI45887

26. Tencerova M, Palmisano B, Lucas S, Attané C, Ivaska KK, Loisay L, Ikushima YM, Trivanovic D, Corsi A, Roque A, Li H, Behler-Janbeck F, Geurts J, Riminucci M, Podgorski I, Cawthorn WP, van der Eerden BCJ, van Wijnen AJ. Experimental analysis of bone marrow adipose tissue and bone marrow adipocytes: An update from the bone marrow adiposity society (BMAS). *Bone Rep*. 2025;26:101861. doi:10.1016/j.bonr.2025.101861

27. Widjaja N, Jalava N, Strauss L, Virtanen KA, Ivaska KK. Supplementary Materials for "Transcriptomic Analysis of Bone Marrow Adipose Tissue Reveals Enrichment in Lipid Transport in Response to Western Diet." *Zenodo*. https://doi.org/10.5281/zenodo.20808825

28. Livak KJ, Schmittgen TD. Analysis of Relative Gene Expression Data Using Real-Time Quantitative PCR and the 2−ΔΔCT Method. *Methods*. 2001;25(4):402-408. doi:10.1006/meth.2001.1262

29. McGrath C, Little-Letsinger SE, Pagnotti GM, Sen B, Xie Z, Uzer G, Uzer GB, Zong X, Styner MA, Rubin J, Styner M. Diet-Stimulated Marrow Adiposity Fails to Worsen Early, Age-Related Bone Loss. *Obes Facts*. 2024;17(2):145-157. doi:10.1159/000536159

30. Muralidharan A, Gomez GA, Kesavan C, Pourteymoor S, Larkin D, Tambunan W, Sechriest VF, Mohan S. Sex-Specific Effects of THRβ Signaling on Metabolic Responses to High Fat Diet in Mice. *Endocrinology*. 2024;165(8). doi:10.1210/ENDOCR/BQAE075

31. Liu LF, Shen WJ, Ueno M, Patel S, Azhar S, Kraemer FB. Age-related modulation of the effects of obesity on gene expression profiles of mouse bone marrow and epididymal adipocytes. *PLoS One*. 2013;8(8). doi:10.1371/JOURNAL.PONE.0072367

32. Subramanian A, Tamayo P, Mootha VK, Mukherjee S, Ebert BL, Gillette MA, Paulovich A, Pomeroy SL, Golub TR, Lander ES, Mesirov JP. Gene set enrichment analysis: a knowledge-based approach for interpreting genome-wide expression profiles. *Proc Natl Acad Sci U S A*. 2005;102(43):15545-15550. doi:10.1073/pnas.0506580102

33. Sárvári AK, Van Hauwaert EL, Markussen LK, Gammelmark E, Marcher AB, Ebbesen MF, Nielsen R, Brewer JR, Madsen JGS, Mandrup S. Plasticity of Epididymal Adipose Tissue in Response to Diet-Induced Obesity at Single-Nucleus Resolution. *Cell Metab*. 2021;33(2):437-453.e5. doi:10.1016/j.cmet.2020.12.004

34. So J, Strobel O, Wann J, Kim K, Paul A, Acri DJ, Dabin LC, Kim J, Peng G, Roh HC. Robust single-nucleus RNA sequencing reveals depot-specific cell population dynamics in adipose tissue remodeling during obesity. *Elife*. 2025;13. doi:10.7554/eLife.97981

35. Wu Y, Sun Y, Chen L, Tong X, Liu C, Lu L, Zhang R, Wang S, Chen Z, Zhang J, Han Z, Zeng B, Li M, Jin L. Dynamics of single-nuclei transcriptomic profiling of adipose tissue from diverse anatomical locations during mouse aging process. *Sci Rep*. 2024;14(1):16093. doi:10.1038/s41598-024-66918-w

36. Widjaja N, Jalava N, Chen Y, Ivaska KK. Perilipin-1 immunostaining improves semi-automated digital quantitation of bone marrow adipocytes in histological bone sections. *Adipocyte*. 2023;12(1). doi:10.1080/21623945.2023.2252711

37. Mairinoja L, Heikelä H, Blom S, Kumar D, Knuuttila A, Boyd S, Sjöblom N, Birkman EM, Rinne P, Ruusuvuori P, Strauss L, Poutanen M. Deep Learning-Based Image Analysis of Liver Steatosis in Mouse Models. *Am J Pathol*. 2023;193(8):1072-1080. doi:10.1016/j.ajpath.2023.04.014

38. Mallick R, Basak S, Das RK, Banerjee A, Paul S, Pathak S, Duttaroy AK. Fatty Acids and their Proteins in Adipose Tissue Inflammation. *Cell Biochem Biophys*. 2024;82(1):35-51. doi:10.1007/s12013-023-01185-6

39. Chavey C, Mari B, Monthouel MN, Bonnafous S, Anglard P, Van Obberghen E, Tartare-Deckert S. Matrix metalloproteinases are differentially expressed in adipose tissue during obesity and modulate adipocyte differentiation. *J Biol Chem*. 2003;278(14):11888-11896. doi:10.1074/jbc.M209196200

40. Bouloumié A, Sengenès C, Portolan G, Galitzky J, Lafontan M. Adipocyte produces matrix metalloproteinases 2 and 9: involvement in adipose differentiation. *Diabetes*. 2001;50(9):2080-2086. doi:10.2337/diabetes.50.9.2080

41. Unal R, Yao-Borengasser A, Varma V, Rasouli N, Labbate C, Kern PA, Ranganathan G. Matrix metalloproteinase-9 is increased in obese subjects and decreases in response to pioglitazone. *J Clin Endocrinol Metab*. 2010;95(6):2993-3001. doi:10.1210/jc.2009-2623

42. Miyaoka Y, Tanaka M, Naiki T, Miyajima A. Oncostatin M inhibits adipogenesis through the RAS/ERK and STAT5 signaling pathways. *J Biol Chem*. 2006;281(49):37913-37920. doi:10.1074/jbc.M606089200

43. Scheller EL, Doucette CR, Learman BS, Cawthorn WP, Khandaker S, Schell B. Region-specific variation in the properties of skeletal adipocytes reveals regulated and constitutive marrow adipose tissues. *Nat Commun*. 2015;6(1). doi:doi:10.1038/ncomms8808

44. Li Z, Hardij J, Bagchi DP, Scheller EL, MacDougald OA. Development, regulation, metabolism and function of bone marrow adipose tissues. *Bone*. 2018;110:134-140. doi:doi:10.1016/j.bone.2018.01.008

45. Tratwal J, Bekri D, Boussema C, Sarkis R, Kunz N, Koliqi T. MarrowQuant Across Aging and Aplasia: A Digital Pathology Workflow for Quantification of Bone Marrow Compartments in Histological Sections. *Front Endocrinol*. 2020;11(480). doi:doi:10.3389/fendo.2020.00480

46. Budzik JF, Lefebvre G, Behal H, Verclytte S, Hardouin P, Teixeira P, Cotten A. Bone marrow perfusion measured with dynamic contrast enhanced magnetic resonance imaging is correlated to body mass index in adults. *Bone*. 2017;99:47-52. doi:10.1016/j.bone.2017.03.048

47. Bartelt A, Koehne T, Tödter K, Reimer R, Müller B, Behler-Janbeck F, Heeren J, Scheja L, Niemeier A. Quantification of Bone Fatty Acid Metabolism and Its Regulation by Adipocyte Lipoprotein Lipase. *Int J Mol Sci*. 2017;18(6):1264-1278. doi:10.3390/ijms18061264

48. Niemeier A, Niedzielska D, Secer R, Schilling A, Merkel M, Enrich C, Rensen PCN, Heeren J. Uptake of postprandial lipoproteins into bone in vivo: impact on osteoblast function. *Bone*. 2008;43(2):230-237. doi:10.1016/j.bone.2008.03.022

49. Hao JW, Wang J, Guo H, Zhao YY, Sun HH, Li YF, Lai XY, Zhao N, Wang X, Xie C, Hong L, Huang X, Wang HR, Li CB, Liang B, Chen S, Zhao TJ. CD36 facilitates fatty acid uptake by dynamic palmitoylation-regulated endocytosis. *Nat Commun*. 2020;11(1):4765. doi:10.1038/s41467-020-18565-8

50. Sun Q, Xing X, Wang H, Wan K, Fan R, Liu C, Wang Y, Wu W, Wang Y, Wang R. SCD1 is the critical signaling hub to mediate metabolic diseases: Mechanism and the development of its inhibitors. *Biomedicine & Pharmacotherapy*. 2024;170:115586. doi:10.1016/j.biopha.2023.115586

51. Ntambi JM, Miyazaki M, Stoehr JP, Lan H, Kendziorski CM, Yandell BS, Song Y, Cohen P, Friedman JM, Attie AD. Loss of stearoyl-CoA desaturase-1 function protects mice against adiposity. *Proc Natl Acad Sci U S A*. 2002;99(17):11482-11486. doi:10.1073/pnas.132384699

52. Picke AK, Sylow L, Møller LL V, Kjøbsted R, Schmidt FN, Steejn MW, Salbach-Hirsch J, Hofbauer C, Blüher M, Saalbach A, Busse B, Rauner M, Hofbauer LC. Differential effects of high-fat diet and exercise training on bone and energy metabolism. *Bone*. 2018;116:120-134. doi:10.1016/j.bone.2018.07.015

53. Huovinen V, Saunavaara V, Kiviranta R, Tarkia M, Honka H, Stark C, Laine J, Linderborg K, Tuomikoski P, Badeau RM, Knuuti J, Nuutila P, Parkkola R. Vertebral bone marrow glucose uptake is inversely associated with bone marrow fat in diabetic and healthy pigs: [(18)F]FDG-PET and MRI study. *Bone*. 2014;61:33-38. doi:10.1016/j.bone.2013.12.022

54. Fazeli PK, Bredella MA, Pachon-Peña G, Zhao W, Zhang X, Faje AT, Resulaj M, Polineni SP, Holmes TM, Lee H, O'Donnell EK, MacDougald OA, Horowitz MC, Rosen CJ, Klibanski A. The dynamics of human bone marrow adipose tissue in response to feeding and fasting. *JCI Insight*. 2021;6(12). doi:10.1172/jci.insight.138636

55. McCabe LR, Irwin R, Tekalur A, Evans C, Schepper JD, Parameswaran N, Ciancio M. Exercise prevents high fat diet-induced bone loss, marrow adiposity and dysbiosis in male mice. *Bone*. 2019;118:20-31. doi:10.1016/j.bone.2018.03.024

56. Scheller EL, Khoury B, Moller KL, Wee NKY, Khandaker S, Kozloff KM, Abrishami SH, Zamarron BF, Singer K. Changes in Skeletal Integrity and Marrow Adiposity during High-Fat Diet and after Weight Loss. *Front Endocrinol (Lausanne)*. 2016;7:102. doi:10.3389/fendo.2016.00102

57. Almeida M, Kim HN, Han L, Zhou D, Thostenson J, Porter RM, Ambrogini E, Manolagas SC, Jilka RL. Increased marrow adipogenesis does not contribute to age-dependent appendicular bone loss in female mice. *Aging Cell*. 2020;19(11):e13247. doi:10.1111/ACEL.13247

58. Iwaniec UT, Turner RT, Iwaniec UT, Turner RT. Influence of body weight on bone mass, architecture and turnover. *Journal of Endocrinology*. 2016;230(3):R115-R130. doi:10.1530/JOE-16-0089

59. Botolin S, McCabe LR. Inhibition of PPARgamma prevents type I diabetic bone marrow adiposity but not bone loss. *J Cell Physiol*. 2006;209(3):967-976. doi:10.1002/JCP.20804

60. Maniglio M, Loisay L, de Haro D, Antoniadis A, Hügle T, Geurts J. Subchondral bone marrow adipose tissue lipolysis regulates bone formation in hand osteoarthritis. *Osteoarthritis Cartilage*. 2025;33(3):322-329. doi:10.1016/j.joca.2024.12.005

61. Chen KC, Sulston RJ, Suchacki KJ, Ikushima YM, Thomas BJ, Lovdel A, Lafond AJ, Mitchell SE, Speakman JR, Morton NM, Semple RK, Cawthorn WP, Chen KC, Sulston RJ, Suchacki KJ, Ikushima YM, Thomas BJ, Lovdel A, Lafond AJ, Mitchell SE, Speakman JR, Morton NM, Semple RK, Cawthorn WP. Caloric restriction exerts site-, sex-, and duration-dependent effects on skeletal structure and bone marrow adiposity. *Journal of Endocrinology*. 2026;269(2):250391. doi:10.1530/JOE-25-0391

62. Kwok KHM, Lam KSL, Xu A. Heterogeneity of white adipose tissue: molecular basis and clinical implications. *Exp Mol Med*. 2016;48(3):e215. doi:10.1038/emm.2016.5

63. Chusyd DE, Wang D, Huffman DM, Nagy TR. Relationships between Rodent White Adipose Fat Pads and Human White Adipose Fat Depots. *Front Nutr*. 2016;3:10. doi:10.3389/fnut.2016.00010

64. Scheller EL, Khandaker S, Learman BS, Cawthorn WP, Anderson LM, Pham HA. Bone marrow adipocytes resist lipolysis and remodeling in response to beta-adrenergic stimulation. *Bone*. 2019;118:32-41.

65. Thrupp N, Sala Frigerio C, Wolfs L, Skene NG, Fattorelli N, Poovathingal S, Fourne Y, Matthews PM, Theys T, Mancuso R, de Strooper B, Fiers M. Single-Nucleus RNA-Seq Is Not Suitable for Detection of Microglial Activation Genes in Humans. *Cell Rep*. 2020;32(13):108189. doi:10.1016/J.CELREP.2020.108189

66. Speakman JR. Use of high-fat diets to study rodent obesity as a model of human obesity. *International Journal of Obesity 2019 43:8*. 2019;43(8):1491-1492. doi:10.1038/s41366-019-0363-7

Figure legends

Figure 1. Phenotypical changes associated with a 12-week Western diet. Analyses of **(A)** body weight, **(B)** body weight gain, **(C)** relative change in whole-body fat fraction, **(D)** non-fasting plasma total cholesterol and **(E)** non-fasting plasma glucose (all N= 15/group). **(F)** Histological analysis of steatotic lesions from whole section of FFPE liver samples (N= 12-13/group). Scale bar: 50 µm, **(G)** Representative 3D renders of humerus microarchitecture evaluated by micro-CT and the analyses of trabecular bone microarchitecture parameters **(H)** trabecular separation (Tb.Sp) and **(I)** trabecular number (Tb.N; all N= 15/group).

Alt text: Graphs and microscopic images labelled A to I. Graphs in A to E depicts the comparison of body weight, weight gain, whole-body fat, plasma total cholesterol and plasma glucose between rats from the chow group and western diet group. F is microscopic images of haematoxylin-eosin-stained liver section with quantitation graph next to it. G is three-dimensional renders of humerus with quantitation graphs in panels H and I.

Figure 2. Collection of BMAT-enriched fraction from tibia and femur. (A) Schematic overview of the separation of stromal-vascular fraction and floating BMAT-enriched fraction by centrifugation, and the presence of bone marrow adipocytes confirmed by staining for neutral lipid and nucleus. Scale bar: 50 µm. (B) Analysis of sample purity by qPCR revealed significantly higher mRNA expression for adipocyte-related markers *Adipoq* and *Plin1*, and significantly lower for haematopoietic-related markers *Ptprc* and *Itgam* in BMAT relative to

the SVF (N= 21). Illustration in (A) is provided by Servier Medical Art (https://smart.servier.com), licensed under CC BY 4.0 (https://creativecommons.org/licenses/by/4.0/).

Alt text: Microscopic image and graph labelled A and B. Panel A shows illustration of sample processing method and a fluorescent microscopic image of acquired sample. Panel B is graph plotting the mRNA expression of various markers in different tissues.

Figure 3. BMAT is a distinct fat depot enriched in transcripts associated with APCs. (A) BMAT expressed significantly less adipocyte-related mRNA *Adipoq, Fabp4, Cd36* and *Leptin* in comparison to WAT and BAT under basal condition without dietary challenge (N= 15/tissue). **(B)** Principal component analysis of BMAT, WAT and BAT transcriptomes, and their representative histological images. Scale bar: 75 µm. Targeted GSEA focusing on the adipocyte physiology pathway-set in **(C)** BMAT versus WAT and **(D)** BMAT versus BAT revealed enrichment in pathways related to membrane lipid processes. **(E)** Analysis of DEGs related to adipoprogenitor cells (upper panel) and preadipocytes (lower panel). Selected gene sets are based on dataset generated from Ambrosi et al. [20]. Verification of select DEGs with qPCR from the whole cohort (N= 14/tissue) on transcripts related to **(F)** adipoprogenitor cells, *e.g.*, *Sca1, Mmp9* and *Osm*, and **(G)** preadipocytes, *e.g., Pref1, Prlr* and *Qprt*.

Alt text: Graphs and microscopic images labelled A to G. A is graph plotting mRNA expression of adiponectin, fabp4, cd36 and leptin in different adipose tissues. B is graph plotting principal component analysis with microscopic images of different adipose tissues

below the graph. C and D are graph plotting normalised enrichment scores of gene ontology-based pathways in different adipose tissues. E is heatmap graph plotting normalised gene expression levels of transcripts related to adipoprogenitor cells and preadipocytes. F and G are graphs plotting the mRNA expression of various markers in different adipose tissues.

Figure 4. A 12-week Western diet significantly increases the size of BMAds and WAds. **(A)** Representative images of humeral bone marrow histological sections, and the average size of BMAds (N= 8-10/group). **(B)** Histogram analysis of the frequency of BMAds, bin width 200 μm^2 between bin centres of 300 μm^2 and 3900 μm^2. **(C)** Representative images of gonadal WAT histological sections, and the average size of WAds (N= 12/group). **(D)** Histogram analysis of the frequency of WAds, bin width 600 μm^2 between bin centres of 600 μm^2 and 8400 μm^2. Scale bars: 75 μm.

Alt text: Graphs and microscopic images labelled A to D. A is microscopy images showing the histology of bone marrow in the chow and western diet group, followed by a graph showing comparison of the size of bone marrow adipocytes. B is a graph plotting the relative frequency of bone marrow adipocytes at different size groups. C is microscopy images showing the histology of gonadal white adipose tissue in the chow and western diet group, followed by a graph showing comparison of the size of white adipocytes. D is a graph plotting the relative frequency of white adipocytes at different size groups.

Figure 5. The expansion of BMAds in Western diet is associated with the enrichment in lipid transport. (A) PCA of BMAT revealed two separated clusters representing BMAT

transcriptomes in the two study groups. **(B)** Transcriptomic analysis revealed 889 DEGs (P_{adj}< 0.05) consisting of 335 upregulated and 554 downregulated DEGs. **(C)** Targeted GSEA limited to the adipocyte physiology pathway-set revealed overall enrichment in several pathways related to lipid transport in the Western diet group (all FDR< 0.25). **(D)** Transcript analysis on those transcripts annotated in the gene ontology-based lipid transport pathway (GO:0006869; all *P*<0.05) in BMAT in control and Western diet groups. Verification of selected DEGs with qPCR from the whole cohort (N= 10-15/group) on transcripts related to lipid transport, *e.g.*, *Cd36*, *Abcg1, Fabp4* and *Acsl4,* in **(E)** BMAT and **(F)** WAT.

Alt text: Graphs and microscopic images labelled A to F. A is graph plotting principal component analysis of the transcriptome of bone marrow adipose tissue from the chow and western diet groups. B is graph showing a volcano plot of statistically significant transcripts from the western diet group in comparison to the chow group, followed by a graph plotting the number of differentially expressed genes that were upregulated and downregulated. C is graph plotting normalised enrichment scores of gene ontology-based pathways in bone marrow adipose tissue upon western diet. D is heatmap graph plotting normalised gene expression levels of transcripts related to lipid transport. E and F are graphs plotting the mRNA expression of various markers in different adipose tissues.

Figure 6. The transcriptomes of BMAT, but not WAT, are enriched in pathways related to the inflammation process upon western diet. Top 10 unfiltered pathways from untargeted GSEA between respective study groups in (A) BMAT and (B) WAT. (C) Transcript analysis on those transcripts annotated in the gene ontology-based immune system process pathway (GO:0002376; all *P*< 0.05). Verification of selected DEGs with PCR from

the whole cohort (N= 10-15/group) on transcripts related to adipocyte-associated immune system process, *e.g.*, *Mcp1, Lcn2, Ccr2, Il1b* and *Il6* in (D) BMAT and (E) WAT.

Alt text: Graphs labelled A to E. A is graph plotting normalised enrichment scores of gene ontology-based pathways in bone marrow adipose tissue upon western diet. B is graph plotting normalised enrichment scores of gene ontology-based pathways in white adipose tissue upon western diet. C is heatmap graph plotting normalised gene expression levels of transcripts related to immune system process. D and E are graphs plotting the mRNA expression of various markers in different adipose tissues.

Figure 7. The expansion of WAds in Western diet is associated with the enrichment in lipid biosynthesis and modification. (A) PCA of WAT revealed two modestly separated clusters representing WAT transcriptomes in the two study groups. **(B)** Transcriptomic analysis revealed 82 DEGs (P_{adj}< 0.05) consisting of 32 upregulated and 50 downregulated DEGs. **(C)** Targeted GSEA limited to the adipocyte physiology pathway-set revealed overall enrichment in pathways related to lipid transport in the Western diet group (all FDR< 0.25). **(D)** Transcript analysis on those annotated in the gene ontology-based lipid biosynthetic process pathway (GO:0008610; all *P*< 0.05) in WAT in control and Western diet groups. Verification of selected DEGs with qPCR from the whole cohort (N= 10-15/group) on transcripts related to lipid biosynthetic process, *e.g.*, *Scd1, Scd2, Pnpla3* and *Lpin3,* in **(E)** WAT and **(F)** BMAT.

Alt text: Graph and microscopic images labelled A to F. A is graph plotting principal component analysis of the transcriptome of white adipose tissue from the chow and

western diet groups. B is graph showing a volcano plot of statistically significant transcripts from the western diet group in comparison to the chow group, followed by a graph plotting the number of differentially expressed genes that were upregulated and downregulated. C is graph plotting normalised enrichment scores of gene ontology-based pathways in white adipose tissue upon western diet. D is heatmap graph plotting normalised gene expression levels of transcripts related to lipid biosynthetic process. E and F are graphs plotting the mRNA expression of various markers in different adipose tissues.

List of tables

Table 1. Humeral length, trabecular and cortical bone microarchitecture parameters and bone mineral density analyses by microCT, and correlation with the size of bone marrow adipocytes.

Parameter [unit]	Chow diet	Western diet	R-coefficient vs. BMAd.Ar	R-coefficient vs, WAd.Ar
Bone length [mm]	30.15 ± 0.23	30.16 ± 0.21	0.455	0.018
Tb.BV/TV [%]	23.63 ± 4.10	21.39 ± 2.34	**-0.480***	-0.047
Tb.N [1/mm]	2.70 ± 0.22	**2.41 ± 0.25****	**-0.673****	-0.124
Tb.Th [mm]	0.087 ± 0.01	0.089 ± 0.59	0.013	0.072
Tb.Sp [mm]	0.372 ± 0.07	**0.50 ± 0.13****	0.288	0.164
Conn.D [1/mm3]	174.79 ± 36.39	**138.93 ± 26.01****	**-0.666****	-0.118
Tb.BMD [g/cm3]	0.95 ± 0.08	0.90 ± 0.12	0.032	-0.200
Ct.Th [mm]	0.352 ± 0.13	0.435 ± 0.16	0.282	0.246
Ct.Po [%]	2.74 ± 1.69	2.30 ± 1.66	-0.116	-0.214
Ct.Ar/Tt.Ar [%]	97.26 ± 1.69	97.70 ± 1.66	0.116	0.214
Ps.Pm [mm]	19.98 ± 3.75	18.28 ± 2.71	-0.073	-0.029
Es.Pm [mm]	14.76 ± 0.62	15.06 ± 0.61	0.061	0.378
Ct.BMD [g/cm3]	1.18 ± 0.11	1.16 ± 0.09	0.287	-0.056

BMAd.Ar= Area of bone marrow adipocyte, WAd.Ar= area of white adipocyte, Tb.BV/TV= trabecular bone volume per tissue volume, Tb.N= trabecular number, Tb.Th= trabecular thickness, Tb.Sp= trabecular

separation, Conn.D= connectivity density, Tb.BMD= trabecular bone mineral density, Ct.Th= cortical thickness, Ct.Po= cortical porosity, Ct.Ar/Tt.Ar= cortical area per tissue area, Ps.Pm= periosteal perimeter, Es.Pm= endosteal perimeter, Ct.BMD= cortical bone mineral density. Data represented as mean ± SD. Groupwise comparison of each parameter was calculated by Student's t-test or Mann-Whitney U-test based on Shapiro-Wilk normality test for data distribution. Correlation coefficient was calculated by Pearson's or Spearmann's correlation based on Shapiro-Wilk normality test for data distribution. *P*-values are presented as **P*<0.05, ***P*<0.01, ****P*< 0.001.

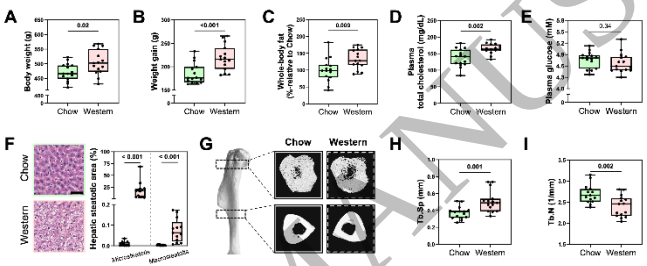

Figure 1
89x36 mm (x DPI)

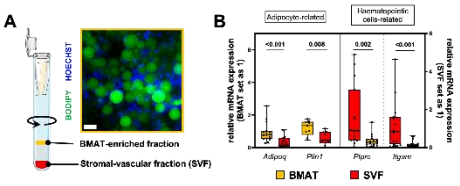

Figure 2
62x25 mm (x DPI)

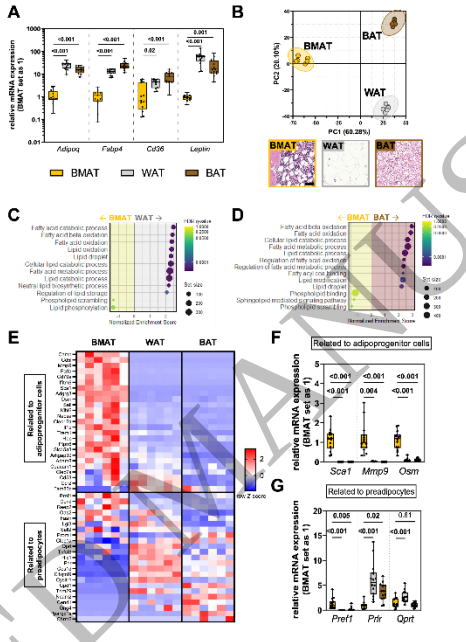

Figure 3
62x84 mm (x DPI)

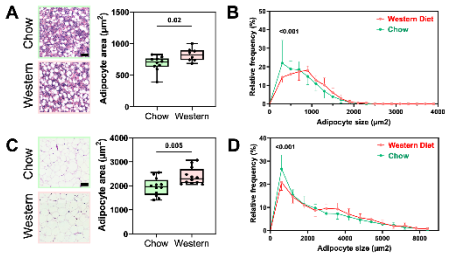

Figure 4
62x35 mm (x DPI)

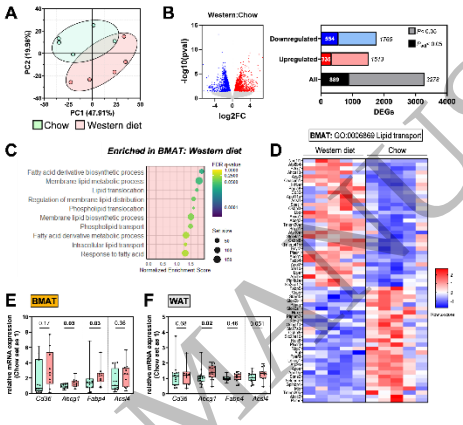

Figure 5
63x54 mm (x DPI)

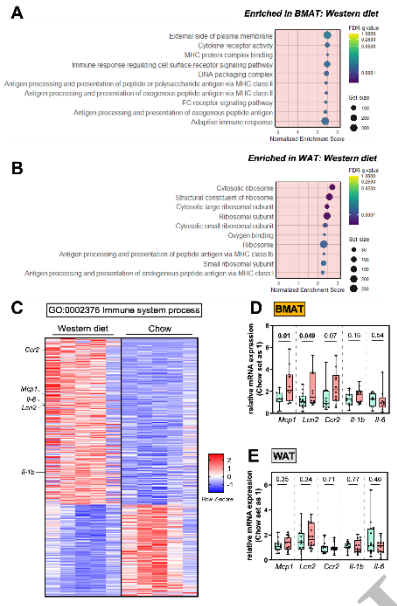

Figure 6
62x80 mm (x DPI)

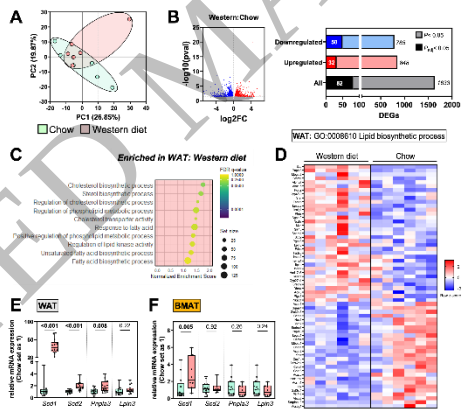

Figure 7
63x54 mm (x DPI)